IL-2 and IL-15 receptor α-subunits are coexpressed in a supramolecular receptor cluster in lipid rafts of T cells

György Vámosi*†, Andrea Bodnár*†, György Vereb‡, Attila Jenei‡, Carolyn K. Goldman§, Jörg Langowski¶, Katalin Tóth¶, László Mátyus‡, János Szöllősi*‡, Thomas A. Waldmann§‖, and Sándor Damjanovich*‡

*Cell Biophysics Research Group of the Hungarian Academy of Sciences and ‡Department of Biophysics and Cell Biology, Research Center for Molecular Medicine, University of Debrecen, Nagyerdei krt. 98, H-4012, Debrecen, Hungary; §Metabolism Branch, Center for Cancer Research, National Cancer Institute, National Institutes of Health, Bethesda, MD 20892; and ¶Division of Biophysics of Macromolecules, Deutsches Krebsforschungszentrum, Im Neuenheimer Feld 580, D-69120 Heidelberg, Germany

Contributed by Thomas A. Waldmann, June 3, 2004

The private α-chains of IL-2 and IL-15 receptors (IL-2R and IL-15R) share the signaling β- and γ_c-subunits, resulting in both common and contrasting roles of IL-2 and IL-15 in T cell function. Knowledge of the cytokine-dependent subunit assembly is indispensable for understanding the paradox of distinct signaling capacities. By using fluorescence resonance energy transfer and confocal microscopy, we have shown that IL-2Rα, IL-15Rα, IL-2/15Rβ and γ_c-subunits, as well as MHC class I and II glycoproteins formed supramolecular receptor clusters in lipid rafts of the T lymphoma line Kit 225 FT7.10. Fluorescence crosscorrelation microscopy demonstrated the comobility of IL-15Rα with IL-2Rα and MHC class I. A model was generated for subunit switching between IL-2Rα and IL-15Rα upon the binding of the appropriate cytokine resulting in the formation of high-affinity heterotrimeric receptors. This model suggests a direct role for the α-subunits, to which no definite function has been assigned so far, in tuning cellular responses to IL-2 or IL-15. In addition, both α-chains were at least partially homodimerized/oligomerized, which could be the basis of distinct signaling pathways by the two cytokines.

IL-2 and IL-15 are critically involved both in innate and adaptive immune responses (1). Their multisubunit receptors share two subunits (β and γ_c) responsible for one set of signal transduction events after ligand binding. In addition, both receptors have their own, "private" α-chains, which presumably ensure the binding of the appropriate cytokine and the specificity of the immune response (2–5). As a result of combining various subunits, several forms of receptor complexes may exist at the cell surface. Biological effects of IL-2 are achieved mainly by its binding to the trimeric, high-affinity IL-2R complex (IL-2R$\alpha\beta\gamma_c$, $K_d \approx 10^{-11}$ M). The IL-15R$\alpha\beta\gamma_c$ complex has a similar high affinity. The $\beta\gamma_c$ heterodimer comprises the intermediate affinity receptor binding IL-2 and IL-15 with similar affinities ($K_d \approx 10^{-9}$ M). Whereas the private IL-2Rα alone binds IL-2 with very low affinity ($K_d \approx 10^{-8}$ M), IL-15Rα is capable of binding IL-15 with a high affinity matching that of the trimeric IL-15R. One signaling pathway shared by both cytokines requires the presence of the β- and γ_c-chains. When this receptor constellation is utilized, IL-2 and IL-15 activate similar janus kinase/signal transducer and activator of transcription (JAK/STAT)-dependent signaling pathways (6).

As anticipated from the sharing of receptor subunits and the use of common elements in one of the signaling pathways, there is significant overlap between the functions of IL-2 and IL-15. Both cytokines can stimulate the proliferation of different subsets of activated T lymphocytes and facilitate the induction of cytolytic effector T cells. In addition to shared functions, IL-2 and IL-15 can also provide distinct and contrasting contributions to T cell-mediated immunity (1). Because IL-2 plays a cardinal role in activation-induced cell death, it is involved in peripheral tolerance through eliminating self-reactive T cells. IL-15, on the other hand, inhibits IL-2-mediated activation-induced cell death. Furthermore, they have opposing roles in the homeostasis of $CD8^+$ memory T cells: Unlike IL-2, IL-15 stimulates the persistence of these cells.

The question arises how cells are able to control the sometimes quite distinct outcomes of biological responses mediated by these cytokines through their very similar receptor composition and signaling machinery. Many alternatives have been suggested to answer this question. IL-15 appears to signal by additional pathways that use IL-15Rα but do not require the expression of β- and γ_c-chains (7, 8). Furthermore, we have demonstrated that, during the induction of the immune response, IL-15Rα and IL-15 are coordinately expressed on the surface of antigen-presenting cells, such as monocytes and dendritic cells. IL-15Rα can present the tightly associated IL-15 in trans to natural killer cells or $CD8^+$ T cells expressing only the β- and γ_c-chains (9). Such trans presentation events occur as part of an immune synapse providing associated costimulatory signals in addition to those initiated by IL-15.

By using fluorescence resonance energy transfer (FRET) techniques we have shown that the three subunits of the high-affinity IL-2R are in the molecular vicinity of each other at the surface of T lymphoma cells even in the absence of IL-2 (10). The addition of IL-2 or IL-15 rearranged the conformation of this preformed receptor complex. In activated and memory T cells where IL-15Rα could be expressed in the same cell as the β- and γ_c-chains, the physical relationship of IL-15Rα to these subunits and IL-2Rα has not been adequately defined. It seems to be plausible that cytokine-specific modulation of subunit assembly, and the consequential alteration of receptor affinity and/or conformation of signaling elements recruited to the receptor complex, might play a role in tuning cellular responses to IL-2 or IL-15. Diversity of downstream signaling may also originate from the different molecular interactions/environments of the two α-chains, which can be manifested through distinct interactions of the two α-chains with the other subunits within the given receptor complexes or their distinct relation to other membrane proteins. Alternatively, the two α-chains may also be accommodated by entirely different membrane regions.

We have previously shown by using FRET and confocal laser scanning microscopy (CLSM) that IL-2R subunits are mainly partitioned into lipid rafts (membrane microdomains rich in sphingolipids and cholesterol) in the plasma membrane of human T lymphoma cells, and we demonstrated that the integrity of lipid rafts has a crucial role in organizing the lateral distribution of IL-2R (11, 12). Integrity of lipid rafts is also essential for IL-2-mediated

Abbreviations: FRET, fluorescence resonance energy transfer; CLSM, confocal laser scanning microscopy; FCS, fluorescence correlation spectroscopy.

†G.V. and A.B. contributed equally to this work.

‖To whom correspondence should be addressed. E-mail: tawald@helix.nih.gov.

www.pnas.org/cgi/doi/10.1073/pnas.0403916101

signaling (12, 13). Lipid rafts may promote the formation and cytokine-specific modulation of IL-2R/IL-15R complexes and β- and γ_c-subunit "switching" between IL-2 and IL-15 receptors.

In the present study, we used FRET and CLSM colocalization measurements to address the subunit assembly and membrane domain localization of IL-15 and IL-2 receptor subunits by using the $CD4^+$ T cell line Kit 225 FT7.10. Because the rate of energy transfer is inversely proportional to the sixth power of the donor–acceptor distance, FRET allows determination of intramolecular or intermolecular distances on the 1- to 10-nm scale (14). On the basis of FRET data, a 2D model describing a possible arrangement of the molecules of interest can be created. On the other hand, CLSM gives information on the lateral distribution of proteins on the few-hundred-nanometer scale, i.e., a second hierarchical level.

FRET and CLSM provide a static picture of intermolecular interactions and molecular distributions. To extend this analysis, in this study we used a dynamic method: fluorescence crosscorrelation spectroscopy (15), which allows the investigation of the joint diffusive motion of distinct molecular species labeled with spectrally different dyes. Thereby, the stability of the interactions can be assessed. The method has an outstanding sensitivity: It is capable of analyzing even single molecules (16).

By using these diverse approaches, we demonstrated that IL-2Rα and IL-15Rα share lipid rafts and are in the molecular vicinity of one another in the human T lymphoma cell line Kit 225 FT7.10. Furthermore, both α-chains formed homodimers/oligomers. A model for the molecular mechanism of β- and γ_c-subunit switching between IL-2 and IL-15 receptors is also proposed.

Materials and Methods

Cell Culture and Cytokine Treatment. Kit 225 FT7.10 and Kit 225 K6 are human T-lymphotrophic virus-nonexpressing, cytokine-dependent (IL-2 or IL-15) human adult T lymphoma cell lines with a $CD4^+$ phenotype derived from Kit 225 cells (17). K6 cells only express mutant IL-15Rα, manifesting a deletion of exons 3 and 4, and FT7.10 cells are transfected with complete IL-15Rα, having an N-terminal FLAG tag. Both cell lines were cultured in RPMI medium 1640 supplemented with 10% FBS, penicillin, and streptomycin. We also added 500 pM human recombinant IL-2 to the medium every 48 h. The medium of FT7.10 cells contained 800 μg/ml G418 (GIBCO) to suppress the growth of WT cells.

In some experiments, the effect of cytokines on the interactions between receptor chains was tested. Freshly harvested FT7.10 cells were washed twice in PBS and then grown in IL-2-free medium for 48 h. Such cells were considered as cells deprived of IL-2. Cells were then washed and incubated in fresh medium with 20 units/ml IL-2 or 100 pM IL-15 for 6 h at 37°C.

Monoclonal Abs. IL-2Rα was targeted with anti-Tac (IgG2a) defining the cytokine-binding epitope or with the noncross-competing 7G7/B6 (IgG2a) mAbs or their Fab fragments. IL-15Rα carrying a FLAG tag was labeled by anti-FLAG M2 (Sigma), whereas the total population of IL-15Rα (transfected ones and native deletion mutants) was labeled with 7A4 24 (IgG2). The IL-2/15Rβ subunits were targeted by Mikβ1 (IgG2a) defining the cytokine-binding epitope or by the noncross-competing Mikβ3 (IgG1κ), whereas the γ_c-chain was targeted by TugH4 mAbs (IgG2b, Pharmingen). Hybridomas producing W6/32 (IgG2aκ) mAb specific for the heavy chain of class I MHC molecules, L368 (IgG1κ) binding β2m, and L243 (IgG2a) binding MHC class II (HLA-DR) were kindly provided by F. Brodsky (University of California, San Francisco). MEM-75 (IgG1) specific for transferrin receptors was a gift from V. Horejsí (Institute of Molecular Genetics, Czech Academy of Sciences, Prague). Aliquots of purified IgGs or Fab fragments were conjugated with succinimidyl esters of Alexa Fluor 488, 546, 568, 633, or 647 dyes (Molecular Probes) or those of Cy3 or Cy5 (Amersham Pharmacia) as described in ref. 18.

Labeling Cells with Fluorescent Markers. Freshly harvested cells were washed twice in ice-cold PBS/0.1% Na-azide, pH 7.4. Azide prevents internalization of IL receptors. The cell pellet was suspended in PBS/azide and incubated with 50 μg/ml fluorescent mAbs or 4–8 μg/ml fluorescent cholera toxin B-subunit (CTX B, Sigma) for 40 min on ice. After being washed, cells were fixed with 1% formaldehyde/PBS. Special care was taken to keep the cells at ice-cold temperature to avoid induced aggregation of cell surface molecules or receptor internalization. For fluorescence correlation spectroscopic experiments, Hanks' balanced salt solution/azide was used, and cells were not fixed to allow diffusion of membrane proteins.

CLSM. CLSM (Zeiss LSM 510) was used for colocalization and acceptor photobleaching FRET measurements. Fluorescently labeled and formaldehyde-fixed cells were mounted on poly-L-lysine-coated coverslips with Mowiol 4–88 (Calbiochem) dissolved in glycerol to reduce unwanted photobleaching. Alexa Fluor 488 was excited at 488 nm; Cy3, Alexa Fluors 546 and 568 were excited at 543 nm; Cy5, and Alexa Fluor 647 were excited at 633 nm. Fluorescence emission was detected through 505- to 550-nm and 560- to 615-nm band-pass filters and 650-nm long-pass filters. Images were taken in MultiTrack mode to prevent cross-talk between the channels. Image stacks of 512 × 512-pixel, 1.0–1.5 μm thick optical sections were obtained with a ×63 Plan-Apochromat oil immersion objective (NA1.4).

Determining Colocalization from Image Crosscorrelation by CLSM. Colocalization of molecules at the few-hundred-nm scale was determined from CLSM images of doubly or triply labeled cells. Two to three optical sections were recorded from the "bottom" (touching the coverslip) or "top" (distal from the coverslip) of the cells. Images were low-pass-filtered to reduce noise, and projection images were created. For a pair of images, x and y, the crosscorrelation coefficient between the intensity distributions of cell-surface labeling was calculated as

$$C = \frac{\sum_{i,j}(x_{ij} - \langle x\rangle)(y_{ij} - \langle y\rangle)}{\sqrt{\sum_{i,j}(x_{ij} - \langle x\rangle)^2 \sum_{i,j}(y_{ij} - \langle y\rangle)^2}}, \qquad [1]$$

where x_{ij} and y_{ij} are fluorescence intensities at pixel coordinates i, j in images x and y, and $\langle x\rangle$, $\langle y\rangle$ are the mean intensities (11). The theoretical maximum is $C = 1$ for identical images, and a value of 0 implies independent localization of the labeled molecules.

Flow Cytometric FRET Experiments. FRET measurements were carried out on a FACSCalibur or a FACSDIVA flow cytometer (Becton Dickinson) as described (19). Briefly, cells were doubly labeled with mAbs tagged with donor (Cy3 or Alexa Fluor 546) or acceptor (Cy5) dyes. Four fluorescence intensities (autofluorescence, donor, FRET, and acceptor channels) were measured from each cell. Excitation/emission occurred at the following wavelengths: 488/530 ± 15 nm, 488/585 ± 21 nm, 488/>670 nm, and 635/661 ± 8 nm with the FACSCalibur and 488/520 ± 10 nm, 532/575 ± 13 nm, 532/>650 nm, and 633/660 ± 10 nm with the FACSDIVA. Cell debris was excluded from analysis by gating on the forward and right angle light scatter signals. List mode files were analyzed as described by using a cell-by-cell autofluorescence correction algorithm to enhance sensitivity (19) with the software FLEX (20). Calculated FRET efficiencies (E) represent the percentage of donor excitation quanta tunneled to acceptor molecules. The mean values of cell-by-cell E histograms were used as characteristic FRET efficiencies between the labeled epitopes.

Pixel-by-Pixel FRET Measurements. Molecular proximity of cell-surface proteins was also investigated by FRET measurements by using the acceptor photobleaching technique. The method (21, 22) is based on the measurement of the enhanced emission of the donor after eliminating FRET by photobleaching the acceptor dye. Single optical sections of the donor (Cy3 or Alexa Fluors 546 or 568) and acceptor (Cy5) intensity distributions from doubly labeled samples were recorded by using low excitation intensities of the 543- and 633-nm laser lines, respectively. Subsequently, acceptor molecules were bleached by repetitive scans with the 633-nm laser line at maximum laser power. After photobleaching, an image of the donor distribution was recorded again. Images were low-pass filtered to reduce noise. Calculations were restricted to those pixels for which the donor intensity was at least the double of the background level measured in a cell-free area. The FRET efficiency E_{ij} at the pixel with coordinates i, j was calculated as

$$E_{ij} = \left(1 - \frac{I_{ij}^{D,pre}}{I_{ij}^{D,post}}\right) \times 100\%\,, \qquad [2]$$

where $I_{ij}^{D,pre}$ and $I_{ij}^{D,post}$ are the background-subtracted donor fluorescence intensities detected before and after photobleaching. Results were presented as pseudocolor FRET efficiency maps and frequency distribution histograms of E_{ij} values.

Fluorescence Correlation Spectroscopy (FCS). In FCS, a focused laser beam excites fluorophores in a subfemtoliter volume element. Diffusion of molecules across this volume causes fluctuations of the fluorescence signal. From the rate of fluctuations, the diffusion coefficient of the molecules can be derived (23). The dual color version of FCS, fluorescence crosscorrelation spectroscopy, can detect joint diffusive motion, i.e., stable association of distinct molecular species (15, 24). The FCS microscope is described in ref. 25. The 488- and 568-nm lines of an Ar–Kr laser focused to diffraction limited spots with intensities of $<0.7\ \mathrm{kW/cm^2}$ were used to excite Alexa Fluor 488 and long-wavelength dyes Alexa Fluor 647 or Cy5, respectively. Fluorescence emission was split by a 570 DRLP dichroic mirror and detected through 515- to 545-nm and 650- to 690-nm band-pass filters by avalanche photodiodes. Spectral separation practically excluded cross-talk between the channels. The instrument can record confocal images and perform FCS measurements at selected points of the sample. Signals are fed into an ALV-5000E correlator card (ALV, Langen, Germany), which calculates the autocorrelation or crosscorrelation function on-line.

Continuous spot illumination caused fast photobleaching of immobile molecules (and molecules within slowly moving molecular aggregates) in the first few seconds. To separate photobleaching phenomena from diffusion processes, runs of 5×3 or 4×4 seconds were recorded, in which the majority of the photobleaching process took place in the first two runs.

Experimental autocorrelation and crosscorrelation functions $G(\tau)$ were fitted to a model function assuming a single molecular species diffusing in 2D (the plane of the plasma membrane) plus a triplet term (26):

$$G(\tau) = \frac{1}{N} \cdot \frac{1 - \Theta_{tr} + \Theta_{tr} e^{-\tau/\tau_{tr}}}{1 - \Theta_{tr}} \cdot \left(1 + \frac{\tau}{\tau_d}\right)^{-1}, \qquad [3]$$

where N is the average number of labeled molecules in the detection volume, Θ_{tr} is the fraction of molecules in the triplet state, τ_{tr} is the phosphorescence lifetime, τ is the lag time, and τ_d is the diffusion correlation time (the mean dwell time of a molecule in the detection volume), which is inversely proportional to the diffusion coefficient. The exact formula describing crosscorrelation between two distinctly labeled species is more complex (15), but its overall shape is very similar. At the signal-to-noise ratio achievable in the cross-correlation measurements of membrane-bound Abs, the above function gave a reasonably accurate fit to the experimental curves.

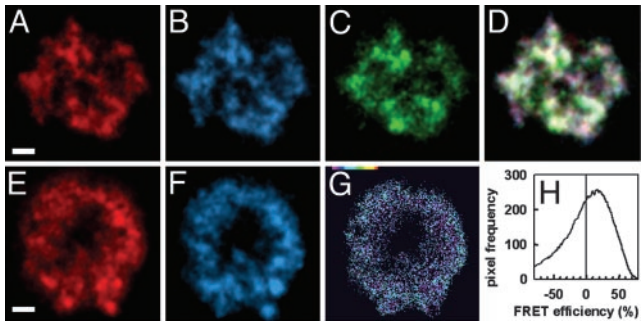

Fig. 1. Triple colocalization of IL-15Rα, IL-2Rα, and lipid rafts and pixel-by-pixel FRET measurement between IL-15Rα and IL-2Rα. (*A–C*) CLSM images of the distribution of IL-15Rα labeled by Cy3-anti-FLAG (*A*), IL-2Rα labeled by Cy5–7G7 B6 (*B*), and lipid rafts labeled with Alexa Fluor 488-CTX B (*C*) recorded from an FT 7.10 cell. (*D*) In the overlay image, white pixels represent colocalization of all three molecules. Pairwise correlation coefficients between the different channels were fairly high (Table 1). (*E* and *F*) Images of IL-15Rα labeled by Cy3–7A4 24, donor (*E*), and IL-2Rα labeled by Cy5-anti-Tac, acceptor (*F*), recorded before acceptor photobleaching. A Pixel-by-pixel FRET efficiency map between IL-15Rα and IL-2Rα (*G*) was determined from the donor images taken before and after photobleaching. The color code ranges between FRET efficiencies of 0% (black) and 100% (red). Pixels with intensities lower than the background threshold appear in black. (*H*) Frequency distribution histogram of FRET efficiencies in the individual pixels. (Scale bar, 2 μm.)

A nonzero crosscorrelation amplitude indicates that at least a certain fraction of the molecules labeled with the spectrally different dyes undergoes joint diffusive motion, i.e., they are stably associated at least for the duration of the diffusion correlation time.

Results

Expression of IL-15 and IL-2 Receptor Subunits. To study the IL-15R, we mainly used Kit 225 FT7.10 cells, a T lymphoma cell line transfected with the gene of IL-15Rα carrying an N-terminal FLAG tag. This cell line also expresses a deletion mutant of IL-15Rα lacking exons 3 and 4, the shared β- and γ_c-chains, and IL-2Rα. Relative cell-surface expressions of these proteins were determined from the mean values of flow cytometric fluorescence intensity histograms of cells labeled with Alexa Fluor 488-conjugated mAbs. The amount of IL-2Rα subunits is ≈5–10 times higher than that of transfected IL-15Rα, and ≈100 times higher than that of the shared IL-2/15Rβ and γ_c. About 60–70% of cells carried the FLAG-tagged gene resulting in >10 times higher expression of IL-15Rα than in nontransfected cells.

Both IL-2Rα and IL-15Rα Are Mainly Partitioned into Lipid Rafts and Have Overlapping Lateral Distributions with Each Other and MHC Glycoproteins. For determining the membrane domain localization of IL-2Rα and IL-15Rα with respect to lipid rafts as well as to each other, cells were triply labeled with fluorescently tagged 7G7 B6 (anti-IL-2Rα), anti-FLAG (anti-IL-15Rα) mAbs, and CTX B, a specific lipid raft marker binding to G_{M1} gangliosides (see Fig. 1). Substantial overlap between the domains rich in IL-2Rα, IL-15Rα, and G_{M1} suggested that the two α-chains were mostly confined to identical lipid rafts. The overlap between the distributions is reflected by the high values of correlation between the pixel intensities in CLSM images (Table 1).

Earlier we found that IL-2R subunits were colocalized with MHC class I and II molecules in the plasma membrane of human T lymphoma cells (11, 12). We were also interested in testing the molecular environment of IL-15Rα in FT7.10 cells. There is an almost perfect overlap between the distributions of IL-15Rα and MHC class I (Fig. 2) or MHC class II (data not shown); the average correlation coefficients determined from CLSM images are ≈0.77 and 0.88, respectively (Table 1). Based on the previous section, this

Table 1. Correlation between pixel intensities of signals arising from pairs of labeled molecules in CLSM images in FT 7.10 cells ($n > 10$)

Labeled epitopes	Label 1	Label 2	Correlation ± SD
IL-15Rα plus IL-2Rα	Cy3-anti-FLAG	Cy5–7G7 B6	0.79 ± 0.06
IL-15Rα plus lipid raft	Cy3-anti-FLAG	Alexa 488-CTX B	0.67 ± 0.08
IL-2Rα plus lipid raft	Cy5–7G7 B6	Alexa 488-CTX B	0.59 ± 0.06
IL-15Rα plus MHC I	Cy3–7A4 24	Cy5-W6/32	0.77 ± 0.08
IL-15Rα plus MHC II	Cy3–7A4 24	Cy5-L243	0.88 ± 0.04
TfR plus lipid raft	Cy3-MEM 75	Cy5-CTX B	0.15 ± 0.10
MHC I HC plus β2m	Cy5-W6/32	Cy3-L368	0.90 ± 0.06

TfR, transferrin receptor; HC, heavy chain; β2m, β2-microglobulin.

result also means that MHC molecules are also mainly localized in lipid rafts in these cells.

Transferrin receptors are localized in coated pits and are excluded from lipid rafts (27). As a negative control, the distribution of transferrin receptors and lipid rafts were compared, resulting in low correlation values ($C = 0.15 \pm 0.1$). As a positive control, the correlation coefficient between the light and heavy chains of MHC class I was determined ($C = 0.9 \pm 0.06$; Table 1).

Probing the Molecular Environment and State of Oligomerization of IL-15Rα Molecules by Flow Cytometric FRET Experiments. FRET measurements were performed to test whether those molecules found in common membrane microdomains with IL-15Rα were also within its 1- to 10-nm environment (the sensitive range of FRET for the applied dyes). The results of flow cytometric cell-by-cell FRET measurements are summarized in Table 2. As a rule-of-thumb, FRET efficiencies >4% can be considered to be significantly different from zero referring to the association of the labeled molecules. Both the IL-2/15Rβ-chains and γ_c-chains showed significant energy transfer with IL-15Rα, implying preassembly of the high-affinity IL-15R even in the absence of IL-15. In addition, significant FRET efficiency was found between IL-15Rα plus IL-2Rα, IL-15Rα plus MHC class I, and IL-15Rα plus MHC class II, indicating nonrandom association of these molecules on FT7.10 cells. The high-FRET efficiency (22.6 ± 2.8%) detected between IL-15Rα subunits implied their at least partial homodimerization/oligomerization on FT7.10 cells.

Earlier we reported that binding of relevant cytokines modulates the interactions between the subunits of IL-2R (10). Therefore, we tested the effect of cytokines on the FRET efficiency between selected receptor subunits in FT7.10 cells. Cells deprived of IL-2 were either treated with IL-2 (20 units/ml for 6 h) or with IL-15 (100 pM for 6 h). Neither IL-2 nor IL-15 caused any significant change in the FRET efficiencies measured between IL-15Rα and IL-2Rα (data not shown). This finding implies that the two distinct α-chains remain associated both in the presence and the absence of the relevant cytokines. Similar measurements were performed to probe the interaction between IL-2/15Rβ (labeled by Cy3-Mikβ3 used as donor) and IL-15Rα (targeted by Cy5–7A4 24 or Cy5-anti-FLAG used as acceptor). Nonzero FRET efficiency was measured among IL-2/15Rβ and IL-15Rα with both acceptor mAbs in untreated and cytokine-treated cells. IL-2 did not significantly affect FRET efficiencies between either donor–acceptor pair. Addition of IL-15 increased E from 4.7 ± 2% to 9.8 ± 3% when using Cy5–7A4 24 as acceptor, whereas it was not altered significantly when using Cy5-anti-FLAG as acceptor (13.2 ± 2% for control versus 11.6 ± 3% for IL-15-treated cells).

Table 2. FRET efficiencies measured by flow cytometry

Labeled epitopes	Donor mAb	Acceptor mAb	E ± SD, %
IL-15Rα and IL-2Rα	Cy3-anti-FLAG	Cy5-anti-Tac	27.5 ± 1.0
	Cy3-anti-FLAG	Cy5–7G7 B6	19.2 ± 2.1
	Cy3–7A4 24	Cy5-anti-Tac	24.4 ± 2.8
	Cy3–7A4 24	Cy5–7G7 B6	15.9 ± 3.0
IL-15Rα and IL-15Rα	Cy3–7A4 24	Cy5–7A4 24	22.6 ± 2.8
IL-15Rα and MHC I	Cy3–7A4 24	Cy5-W6/32	33.4 ± 3.1
IL-15Rα and β2m	Cy3–7A4 24	Cy5-L368	34.4 ± 3.0
IL-15Rα and MHC II	Cy3–7A4 24	Cy5-L243	56.6 ± 6.1
IL-2/15Rβ and IL-15Rα	Cy3-Mikβ3	Cy5-anti-FLAG	13.2 ± 4.0
	Cy3-Mikβ3	Cy5–7A4 24	4.7 ± 2.2
γc and IL-15Rα	Alexa 546-TUGH4	Cy5–7A4 24	10.6 ± 1.8
	Alexa 546-TUGH4	Cy5-anti-FLAG	14.6 ± 1.3
IL-2Rα and MHC I	Cy3-anti-Tac	Cy5-W6/32	30.5 ± 1.1
IL-2Rα and MHC II	Cy3-anti-Tac	Cy5-L243	44.9 ± 0.3

Data represent mean ± SD values of at least three measurements.

Microscopic Pixel-by-Pixel FRET Experiments. Spatial distribution of the FRET efficiency between labeled proteins was visualized by CLSM by using the acceptor photobleaching technique (21). It was confirmed that IL-15Rα is colocalized at the molecular level with IL-2Rα, MHC class I, and MHC class II in FT 7.10 cells. Representative FRET efficiency maps and histograms are shown in Figs. 1 and 2. The rather homogenous character of the FRET efficiency map (Fig. 2) indicates that MHC class I (and MHC class II) molecules are in the vicinity of IL-15Rα throughout the membrane domains containing IL-15Rα.

Significant FRET efficiency (≈20%) was measured between IL-2/15Rβ and IL-15Rα labeled by Alexa Fluor 568-Mikβ1 and Cy5–7A4 24 on FT 7.10 cells (image not shown), corroborating the finding of flow cytometric analysis and indicating molecular association of these subunits.

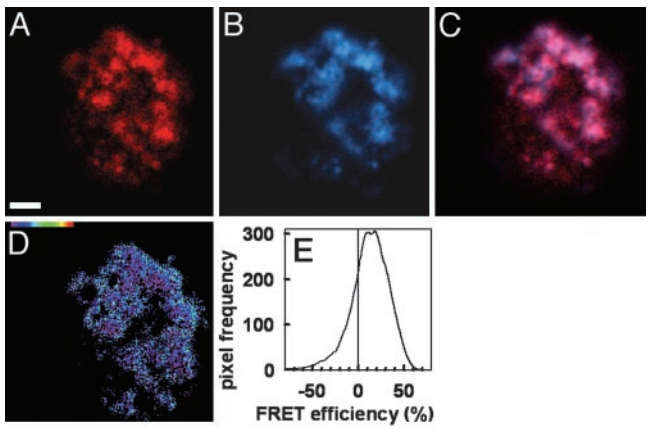

Fig. 2. Colocalization and pixel-by-pixel FRET between IL-15Rα and MHC class I on FT 7.10 cells. (*A* and *B*) CLSM images of the distribution of IL-15Rα labeled with Cy3–7A4 24 (*A*) and MHC class I labeled with Cy5-W6/32 (*B*). (*C*) The overlay is pink where overlap is significant. The correlation coefficient was $C = 0.77$. In the pixel-by-pixel FRET efficiency map between IL-15Rα and MHC class I (*D*) the color code ranges between 0% (black) and 100% (red). (*E*) Frequency distribution histogram of FRET efficiencies in the individual pixels. (Scale bar, 2 μm.)

Homodimerization of IL-2Rα was studied by labeling with Cy3-anti-Tac and Cy5-anti-Tac mAbs simultaneously. On FT 7.10 cells, a relatively high FRET efficiency was detected with histograms peaking around $E = 15\%$. In agreement with earlier data (28), on Kit 225 K6, a distinct subline of Kit 225 cells, mean FRET efficiencies did not significantly differ from 0 ($E = 0$–4%).

Mobility and Comobility Measurements by FCS: Both IL-15Rα and IL-2Rα Are Associated with MHC Class I and with One Another. FRET measurements on fixed cells record a snapshot of interactions between labeled molecules over a large ensemble. In contrast, FCS is a dynamic method capable of demonstrating that interacting molecules diffusing across a small confocal volume element form stable complexes remaining together at least on the time scale of the diffusion correlation time.

The comobility of IL-15Rα, IL-2Rα, and MHC class I was studied in FT 7.10 cells. Positive crosscorrelation amplitude was obtained between IL-15Rα and IL-2Rα (labeled by Alexa Fluor 488-anti-FLAG mAb and Cy5-anti-Tac Fab) in ≈20% of the cases, whereas IL-15Rα and MHC class I (labeled with Alexa Fluor 488-anti-FLAG and Cy5-W6/32) yielded positive crosscorrelation amplitudes in ≈80% of all cases. In K6 cells IL-2Rα and MHC class I (labeled by Alexa Fluor 488-anti-Tac Fab and Cy5-W6/32) showed nonzero crosscorrelation in ≈80% of the cases (see Fig. 3). These findings are in agreement with the positive FRET results and suggest that the studied molecular complexes are stable on a time scale of at least several tens of milliseconds, the diffusion correlation time.

As a positive control, MHC class I molecules labeled with W6/32 mAbs conjugated with both Alexa Fluor 488 and 647 were used on FT 7.10 cells and resulted in positive crosscorrelation. No crosscorrelation could be detected between transferrin receptors and IL-2Rα molecules labeled by Alexa Fluor 488-MEM75 and Cy5-anti-Tac mAbs on K6 cells (negative control).

Discussion

Understanding the molecular details of signaling by IL-2 and IL-15 requires the knowledge of the structure and interactions of their multisubunit receptors. A major focus of our efforts was therefore to investigate the topology of the IL-2/IL-15 receptor system consisting of the shared β- and γ_c-subunits and the distinct IL-2Rα- and IL-15Rα-chains.

In the present study, we used the $CD4^+$ leukemia T cell line Kit 225 FT7.10 to define whether the three subunits of the IL-15R can be expressed in the same membrane domain. Our flow cytometric and confocal microscopic FRET measurements unequivocally demonstrated the molecular proximity of IL-15Rα to β- and γ_c-chains. Thus, the three subunits of IL-15R usually occur in the same lipid domain and are molecularly associated (preassembled) in FT7.10 cells. Such an association in the same domain is supported by our observations made in the cytokine-dependent natural killer cell line NK-92, which can respond by proliferation to picomolar concentrations of IL-15, implying that IL-15Rα is coexpressed in association with the other IL-15R subunits (T.A.W., unpublished data). Furthermore, as part of the study of the efficacy of HIV vaccine vectors, we demonstrated that, during the late phases of the evolution of the immune response, 64% of the splenic $CD8^+$ T cells of the mice receiving a vaccine encoding IL-15 expressed IL-15Rα (29). Such $CD8^+$ T cells induced *in vivo* with IL-15-containing vaccines expressed IL-15Rα and proliferated better *ex vivo* than those generated with control vaccines not expressing IL-15. On the basis of these studies we suggest that, during the evolution of the immune response, coexpression of all three elements of the IL-15R in the same membrane domain occurs in mature memory T cells in addition to trans presentation by membrane-assembled IL-15Rα and IL-15 on antigen-presenting cells that occurs at the initiation of the immune response. Such coexpression in responding T cells may be involved in the maintenance of long-term $CD8^+$ memory responses.

IL-2 and IL-15 invoke similar cellular responses in many cases, but they also have opposite effects on the life and death of lymphocytes. A number of molecular mechanisms may underlie this bifurcation of signaling capacities. IL-2 acts as a soluble factor that functions by interacting with a heterotrimeric IL-2R expressed on a single cell. In contrast, in select circumstances IL-15 expressed in association with IL-15Rα on antigen-presenting cells interacts as part of an immune synapse with a second cell, e.g., a cytokine-responsive natural killer or memory T cell. These observations suggest that IL-15 on antigen presentation functions as a costimulatory molecule along with an array of other stimulatory signals, including those mediated by the interaction of the MHC–antigen complex with the T cell receptor, CD80/86 with CD28, or the CD40 ligand with CD40.

It is conceivable that in cells expressing all elements of the IL-15 and IL-2 receptors, the distinct α-subunits of IL-15R and IL-2R may reside in different membrane domains and molecular environments. However, according to our results, in the T lymphoma cells of the present study any effects of cytokines could not be based on the localization of IL-2Rα and IL-15Rα in completely different compartments. By using CLSM, IL-2Rα and IL-15Rα were found to be strongly colocalized on the ≈200-nm scale in G_{M1}-rich membrane microdomains (Table 1 and Fig. 1), implying that IL-2 and IL-15 mainly fulfill their function in lipid rafts in FT7.10 cells. The high FRET efficiency between IL-15Rα and IL-2Rα (Table 2) suggests their association at the molecular level as well. Our previous studies with different T lymphoma cells indicated that the multisubunit IL-2R complex is associated with MHC class I, MHC class II, and intercellular adhesion molecule-1 coexpressed in lipid rafts (11, 12, 30). In this study, the domain-level colocalization and molecular proximity of IL-15Rα to MHC class I and II molecules were shown. In summary, our experiments revealed considerable similarity between the direct molecular environments of IL-2Rα and IL-15Rα in Kit 225 FT7.10 cells. Yet it is possible that, although the subunits reside in identical microdomains, IL-2R and IL-15R could differentially interact with downstream signaling molecules.

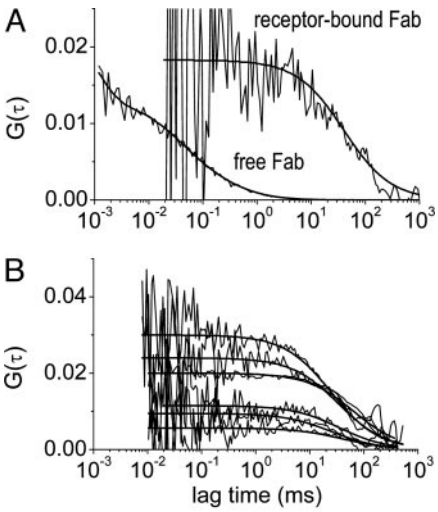

Fig. 3. Fluorescence correlation curves detected from IL-2Rα and MHC class I labeled by Alexa 488-anti-Tac Fab and Cy5-W6/32 on Kit 225 K6 cells. (*A*) Autocorrelation curve detected from Alexa 488-anti-Tac Fabs free in solution and bound to IL-2Rα. Comparison of the correlation times implies that the diffusion coefficient of the free Fab is approximately three orders of magnitude larger than that of the receptor-bound one. (*B*) Crosscorrelation curves demonstrating the association of MHC class I (labeled by Cy5-W6/32) with IL-2Rα, which is stable at least on the time scale of the diffusion crosscorrelation time (48 ± 23 ms).

In addition to the pathways involving the shared β- and γ_c-chains, there is emerging evidence for $\beta\gamma_c$-independent signaling pathways mediated by the interaction of IL-15 with IL-15Rα alone (7, 8). In analogy with other growth factors, such a pathway may involve receptor homodimerization. Indeed, our FRET experiments indicated the homodimeric/oligomeric molecular association of IL-15Rα. In this and previous (28) studies, we have shown that homoassociation of IL-2Rα may also occur in T lymphoma cells, although in a cell-type-dependent manner. Homoassociation of IL-15Rα may also enhance the efficiency of trans presentation in intercellular signaling.

Previously we have shown the preassembly of the three IL-2R subunits on resting Kit 225 K6 T cells (10). Here we demonstrated a similar preassembly of IL-15R and the colocalization of IL-15Rα with IL-2Rα, MHC class I, and MHC class II in lipid rafts. This nonrandom relationship of IL-15Rα with the other elements of the IL-2R cluster is supported by our previous observation (10) that the addition of IL-2 to K6 cells strengthened the bridges among the IL-2R subunits, making the triangle among these subunits more compact. In contrast, addition of IL-15 acted in the opposite direction by opening the triangle, possibly because IL-15Rα associated with the shared γ_c- and/or β-chains and thus diverted them from IL-2Rα. A similar distancing of γ_c from IL-2Rα was observed when IL-7 was added. In this study, we showed that FRET efficiency between the β-chain and IL-15Rα increased upon binding IL-15, suggesting that interaction between these subunits became tighter, whereas the FRET efficiency between IL-15Rα and IL-2Rα remained unchanged. Based on these data, a tetrameric IL-2/IL-15 receptor complex can be envisaged (Fig. 4). In this model, which is in accordance with both our previous model of the heterotrimeric IL-2R complex (10) and our new observations, binding of the appropriate cytokine rearranges the receptor subunits to form a high-affinity receptor trimer ($\alpha\beta\gamma_c$), whereas the "unused" α-chain rotates or shifts away from the site of cytokine–receptor interaction. This arrangement would make the use of the relatively weakly expressed shared β- and γ_c-subunits by the private α-chains highly efficient and economical. Furthermore, upon binding of the appropriate cytokine, the conformation of the receptor complex could quickly shift and result in modifying the assembly of intracellular signal molecules. The proposed mechanism suggests a direct role for the two α-chains, to which no definite function has been assigned so far, in tuning cellular responses to IL-2 or IL-15. Compartmentation of the receptor chains by lipid rafts may assist in setting up the proper conformation of the heterotetrameric complex.

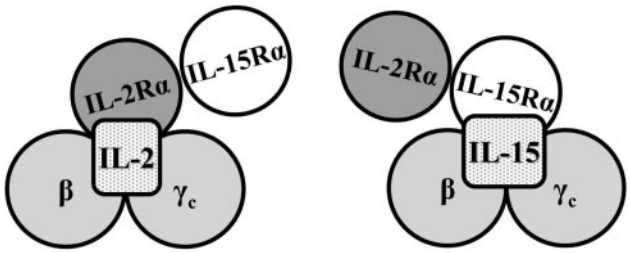

Fig. 4. A possible model of the IL-2/IL-15 receptor complex. FRET data presented in this paper and previous studies on the IL-2R alone (10) are compatible with a tetrameric structure of the IL-2/IL-15 receptor complex. IL-2Rα and IL-15Rα are in the molecular vicinity of each other in the presence and absence of cytokines as well. Binding of IL-2 or IL-15 leads to an increase of FRET efficiency between the IL-2/15Rβ and IL-2Rα or IL-15Rα, respectively. These observations could be explained by the coordinated rotational/translational motion of the IL-2Rα and IL-15Rα subunits with respect to the $\beta\gamma_c$ heterodimer.

As an extension of this model, our observations suggest the possibility of a supercomplex of MHC, intercellular adhesion molecule-1, and cytokine receptor subunits that could include all members of the γ_c cytokine receptor family in addition to IL-2Rα, in particular, IL-4Rα, IL-7Rα, IL-9Rα, IL-15Rα, and IL-21Rα. Such an association in a lipid-raft-accommodated supercomplex could provide one explanation for the functional competition among cytokines that has been observed upon the simultaneous addition of IL-2 and IL-4 to lymphocytes. Furthermore, the definition of such a supercomplex of cytokine receptors would add to our understanding of the regulation of lymphocyte proliferation and effector immune responses that are mediated by these pivotal γ_c-associated cytokines.

We thank Ms. R. Szabó for excellent technical assistance. This work was supported by Hungarian National Research Fund Grants TS40773, T42618, F46497, T37831, F34497, T43061, T43509, ETT 117/2001, 602/2003, 603/2003, and 524/2003; North Atlantic Treaty Organization Life Science and Technology Collaborative Linkage Grant 980200; Bolyai János Research Fellowships (to G.V. and A.B.); and a Békésy György Postdoctoral Fellowship (to G.V.).

1. Waldmann, T. A., Dubois, S. & Tagaya, Y. (2001) *Immunity* **14,** 105–110.
2. Nakamura, Y., Russell, S. M., Mess, S. A., Friedmann, M., Erdos, M., Francois, C., Jacques, Y., Adelstein, S. & Leonard, W. J. (1994) *Nature* **369,** 330–333.
3. Nelson, B. H. & Willerford, D. M. (1998) *Adv. Immunol.* **70,** 1–81.
4. Tagaya, Y., Bamford, R. N., DeFilippis, A. P. & Waldmann, T. A. (1996) *Immunity* **4,** 329–336.
5. Fehniger, T. A. & Caligiuri, M. A. (2001) *Blood* **97,** 14–32.
6. Lin, J. X., Migone, T. S., Tsang, M., Friedmann, M., Weatherbee, J. A., Zhou, L., Yamauchi, A., Bloom, E. T., Mietz, J., John, S., *et al.* (1995) *Immunity* **2,** 331–339.
7. Bulanova, E., Budagian, V., Pohl, T., Krause, H., Durkop, H., Paus, R. & Bulfone-Paus, S. (2001) *J. Immunol.* **167,** 6292–6302.
8. Dubois, S., Shou, W., Haneline, L. S., Fleischer, S., Waldmann, T. A. & Muller, J. R. (2003) *Proc. Natl. Acad. Sci. USA* **100,** 14169–14174.
9. Dubois, S., Mariner, J., Waldmann, T. A. & Tagaya, Y. (2002) *Immunity* **17,** 537–547.
10. Damjanovich, S., Bene, L., Matkó, J., Alileche, A., Goldman, C. K., Sharrow, S. & Waldmann, T. A. (1997) *Proc. Natl. Acad. Sci. USA* **94,** 13134–13139.
11. Vereb, G., Matkó, J., Vámosi, G., Ibrahim, S. M., Magyar, E., Varga, S., Szöllősi, J., Jenei, A., Gáspár, R., Jr., Waldmann, T. A. & Damjanovich, S. (2000) *Proc. Natl. Acad. Sci. USA* **97,** 6013–6018.
12. Matkó, J., Bodnár, A., Vereb, G., Bene, L., Vámosi, G., Szentesi, G., Szöllősi, J., Gáspár, R., Horejsi, V., Waldmann, T. A. & Damjanovich, S. (2002) *Eur. J. Biochem.* **269,** 1199–1208.
13. Marmor, M. D. & Julius, M. (2001) *Blood* **98,** 1489–1497.
14. Stryer, L. & Haugland, R. P. (1967) *Proc. Natl. Acad. Sci. USA* **58,** 719–726.
15. Weidemann, T., Wachsmuth, M., Tewes, M., Rippe, K. & Langowski, J. (2002) *Single Molecules* **3,** 49–61.
16. Medina, M. A. & Schwille, P. (2002) *BioEssays* **24,** 758–764.
17. Hori, T., Uchiyama, T., Tsudo, M., Umadome, H., Ohno, H., Fukuhara, S., Kita, K. & Uchino, H. (1987) *Blood* **70,** 1069–1072.
18. Szöllösi, J., Horejsi, V., Bene, L., Angelisova, P. & Damjanovich, S. (1996) *J. Immunol.* **157,** 2939–2946.
19. Sebestyén, Z., Nagy, P., Horváth, G., Vámosi, G., Debets, R., Gratama, J. W., Alexander, D. R. & Szöllösi, J. (2002) *Cytometry* **48,** 124–135.
20. Szentesi, G., Horváth, G., Bori, I., Vámosi, G., Szöllősi, J., Gáspár, R., Damjanovich, S., Jenei, A. & Mátyus, L. (2004) *Comp. Meth. Prog. Biomed.*, in press.
21. Bastiaens, P. I., Majoul, I. V., Verveer, P. J., Soling, H. D. & Jovin, T. M. (1996) *EMBO J.* **15,** 4246–4253.
22. Vereb, G., Meyer, C. K. & Jovin, T. M. (1997) in *Interacting Protein Domains: Their Role in Signal and Energy Transduction*, NATO ASI Series, ed. Heilmeyer, L. M. G., Jr. (Springer, New York), Vol. H102, pp. 49–52.
23. Elson, E. & Magde, D. (1974) *Biopolymers* **13,** 1–27.
24. Bacia, K. & Schwille, P. (2003) *Methods* **29,** 74–85.
25. Wachsmuth, M., Weidemann, T., Muller, G., Hoffmann-Rohrer, U. W., Knoch, T. A., Waldeck, W. & Langowski, J. (2003) *Biophys. J.* **84,** 3353–3363.
26. Widengren, J., Mets, Ü. & Rigler, R. (1995) *J. Phys. Chem.* **99,** 13368–13379.
27. Harder, T., Scheiffele, P., Verkade, P. & Simons, K. (1998) *J. Cell Biol.* **141,** 929–942.
28. Eicher, D. M., Damjanovich, S. & Waldmann, T. A. (2002) *Cytokine* **17,** 82–90.
29. Oh, S., Berzofsky, J. A., Burke, D. S., Waldmann, T. A. & Perera, L. P. (2003) *Proc. Natl. Acad. Sci. USA* **100,** 3392–3397.
30. Bene, L., Balázs, M., Matkó, J., Most, J., Dierich, M. P., Szöllősi, J. & Damjanovich, S. (1994) *Eur. J. Immunol.* **24,** 2115–2123.